Particle Accelerators, 1992, Vols. 37–38, pp. 371–384
Reprints available directly from the publisher
Photocopying permitted by license only

INTENSE BEAM-TARGET INTERACTION EXPERIMENTS WITH HEAVY IONS

D. H. H. HOFFMANN, K.-G. DIETRICH, W. LAUX, E. BOGGASCH[1], J. JACOBY[1], K. MAHRT-OLT[1], A. TAUSCHWITZ[1], B. HEIMRICH[2], M. WINKLER[2] and P. SPILLER[2]

GSI-Darmstadt, Postfach 110552, 6100 Darmstadt, Germany

(Received 25 January 1991)

Heavy ion beams from the new accelerator facility SIS/ESR at GSI Darmstadt are now available for experiments with energies exceeding 1 GeV/u. Using intense beam pulses of $\geq 10^9$ particles per pulse in 100 ns it will soon be possible to produce high density beam driven plasmas. The aim of the research program is to investigate interaction processes of intense heavy ion beams with hot ionized matter. A new fine focus system has been designed to produce a high deposition power beam for target experiments with a beam spot radius of 100 μm. Nonconventional focusing devices such as plasma lenses will further improve the power deposition of the beam.

The low intensity beam from the GSI UNILAC has been used to measure the energy loss of heavy ions in a fully ionized hydrogen plasma. A strong enhancement of the stopping power for heavy ions in a plasma environment has been observed.

1 INTRODUCTION

Ion beam driven fusion today is viewed as a competitive alternative route to energy production from thermonuclear fusion processes. Commercial power production requires a highly efficient and reliable driver. Particle accelerators, with their high efficiency ($\geq 25\%$) and proven reliability, as well as their ability to deliver high intensity beam pulses at a high repetition rate (≥ 1 Hz), are likely to match the driver requirements for inertial fusion energy (IFE) production.

The demands on a heavy ion driver are, however, very severe if we consider for a moment the key figures that are involved in ion driven fusion. It is expected that the energy delivered to the target in a 10 ns pulse has to be in the range of 5 to 10 MJ, which amounts to a pulsed power of 10^{15}W. The symmetry requirements of ICF pellets during the heating and compression process are difficult to meet with directly driven targets; this makes it appear likely that the indirect drive approach will be pursued. In this case it is necessary to heat a hohlraum to temperatures of approximately 300 eV to obtain a circulating flux of 10^{15} W/cm^2. Thus the ion beam kinetic energy has to be absorbed and converted into thermal radiation in a small amount

[1] Max-Planck-Institut für Quantenoptik, Garching, Germany.
[2] II. Physikalisches Institut, Justus-Liebig-Universität Giessen, Germany.

of matter. Using these figures the order of magnitude for the deposition power P_ρ (measured in W/g), which is the key parameter for heating matter with heavy ion beams, can be estimated to be 10^{16} W/g. The advanced state of present day accelerator technology, and novel techniques and ideas to produce high intensity beam pulses[1], suggest that this parameter regime can be reached in the near future if a vigorous international research effort is pursued.

Recent advances in high power laser development make it appear likely that a laser driver will be the first device to ignite a fusion pellet under laboratory conditions and achieve gain.[2] Therefore it is reasonable, for an indirect drive scenario, that target and implosion physics issues will be studied experimentally using the advanced laser facilities as they become available, whereas intense heavy ion beams should be investigated for their potential to heat a converter material efficiently to high temperatures as required for an indirectly driven fusion pellet.

2 HIGH ENERGY DENSITY IN MATTER INDUCED BY HEAVY ION BEAMS

An experimental program to investigate beam plasma interaction phenomena was initiated at GSI some years ago[3], when it became clear that the accelerator facilities at GSI would provide the most powerful heavy ion beams worldwide and offer outstanding experimental conditions to address key issues of inertial confinement fusion. The entire experimental program was geared to lay the foundations for a dedicated research program using the new accelerator scenario consisting of the SIS and ESR (Figure 1), and a high current injector for UNILAC which will be added in 1992.

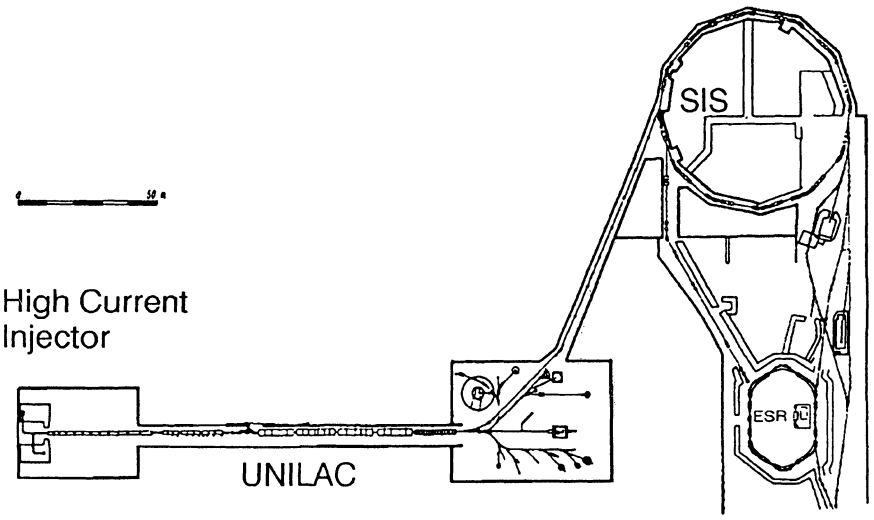

FIGURE 1 Accelerator facilities at GSI. The UNILAC injects into the heavy ion synchroton (SIS) and the experimental storage ring (ESR). At the right hand side is the target cave for intense beam experiments. A high current injector for the UNILAC will be installed after 1992.

Heavy ion beams from the SIS are now available for experiments, and all ions provided by the UNILAC with an intensity of at least 1 μA electrical pulse current can be accelerated up to the design energy[4]. Currently the maximum number of particles per pulse for light ions like neon or argon is in the 10^8 range, but we expect the machine soon to deliver 10^9 particles per pulse in 100 ns. With this beam focused on a small sample of matter, it will then be possible to produce a high density plasma with intense heavy ion beams, investigate interaction processes of heavy ions with hot ionized matter, and addresses key issues of inertial confinement fusion (ICF).

The potential of heavy ion beams to heat matter to extreme conditions of temperature and pressure is expressed by the deposition power P_ρ:

$$P_\rho = (E \times I)/(a \times r) \qquad [\mathrm{TW/g}] \tag{1}$$

with the total particle energy (E), the particle intensity (I), the focal spot area (a), and the range of the ion beam in matter (r). Improvement of the focal spot area by advanced focusing techniques and the investigation of energy deposition profiles of heavy ions in ionized matter are research subjects of the experimental program at GSI.

2.1 High Energy Density Target Area at SIS

For the intense beam-target experiments the high energy density (HED) target area has been designed (Figure 2). Beam pulses of maximum intensity from the SIS, bunched to 100 ns pulse length, are focused to a spot size of about 100 μm radius by a lens array of five magnetic quadrupoles. In the early operating phase of SIS the maximum intensity for Ne^{3+} pulses will be merely above 10^9 particles at 300 MeV/u, which is just sufficient for a well focused beam to heat the target spot to 1 eV for high Z material and a few eV for low density material.

New diagnostic techniques specific to ion beam induced plasmas have been developed during the intense beam experiments at the RFQ accelerator, and the experimental equipment will now be set up at the new experimental area. A major aim of the experiments is to understand the hydrodynamic response of the target material and compare this to numerical simulations[5]. Therefore the target response will be diagnosed by means of optical and x-ray spectroscopy to measure time and

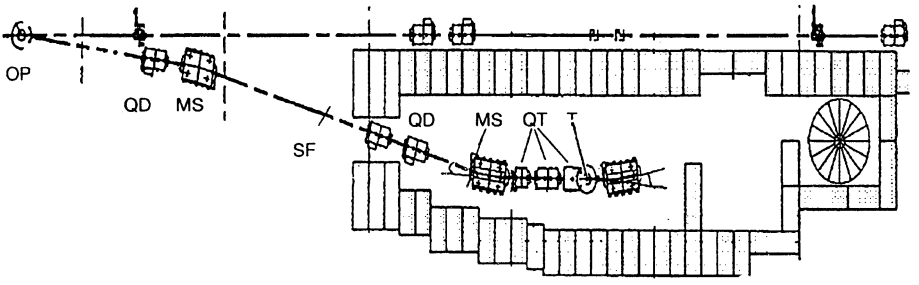

FIGURE 2 Final focus system at the Target area for intense beam experiments (OP = takeover point; MS = magnetic sector; SF = stripper point; QD = quadrupole doublet; QTl = quadrupole triplet; T = target).

space resolved spectral emission of the expanding target. For this purpose the spectrometers are coupled to high resolution streak cameras with digital readout systems (CCD cameras). One specific way to analyze density fluctuations of the expanding target is to measure the energy loss of the ions after target passage. A spectrometer consisting of a dipole magnet for momentum dispersion and a position sensitive detector (PSD) is currently being designed by a group of the IPN (Orsay), and will be available for experiments to measure the energy loss of heavy ions in beam heated plasmas.

Centerpiece of the experimental set-up is the final focus system[6], which achieves the smallest possible focal spot size of the beam. The design of the system has been calculated with the GIOS code[7], assuming the following beam parameters: emittance $\varepsilon = 1.5\ \pi$ mm mrad, momentum spread $\Delta p = 0.4\%$, and beam energy $E/A = 300$ MeV/u. In Figure 2, the magnetic beam guidance system from the takeover point (OP) to the focal spot at the target (T) is shown.

From the takeover point up to the stripper foil (SF), the magnetic system is designed to handle beam pulses up to the maximum value of the magnetic rigidity of 18 T-m. Downstream of the stripper foil the charge state of the ions is increased ($Ne^{3+} \rightarrow Ne^{10+}$), and the demands on the focusing system are reduced to a maximum magnetic rigidity of 6 T-m, which is necessary to keep the magnetic flux density of the last quadrupole below 0.7 T. The electrical beam current, however, increases by the same factor, causing space charge effects to play a more important role, and up to 10% of the focusing power is used to compensate for space charge effects.

2.2 *Advanced Focusing Techniques*

The success of high power lasers in ICF applications is due to the fact that laser light can be focused extremely well in space and time simultaneously. New focusing techniques using plasma lenses hold the promise that also intense heavy ion beams can be focused to very small spot sizes.

In the early phase of our experimental program studying interaction phenomena of heavy ion beams with plasma targets, we were already aware of plasma effects in our z-pinch discharge[7]. Figure 3 shows the beam intensity signal observed during a plasma discharge in front and behind the z-pinch target. While the intensity is constant during the discharge process in front of the target, we observe a strong variation of the transmitted beam intensity and finally even an enhanced transmission. Using a Monte-Carlo code we were able to simulate the focusing properties of the plasma target. Figure 4 shows the result of this computer simulation for an Ar^{10+} beam of 11.4 MeV/u. A parallel beam is incident on the entrance aperture of the plasma target. Due to the radial magnetic field gradient (25 T/m) associated with the pinch current of some 10 kA the beam is focused behind the plasma target. The figure shows the trajectories of 30 particles (Ar^{10+}, $E_o = 11.4$ MeV/u). Collisions and charge exchange processes of the beam projectiles led to a statistical distribution of the projectile position at the target exit. The average charge state after passing the plasma target is 16+. We regard focusing of intense heavy ion beams by non conventional methods like plasma lenses as a very promising way to increase the deposition power

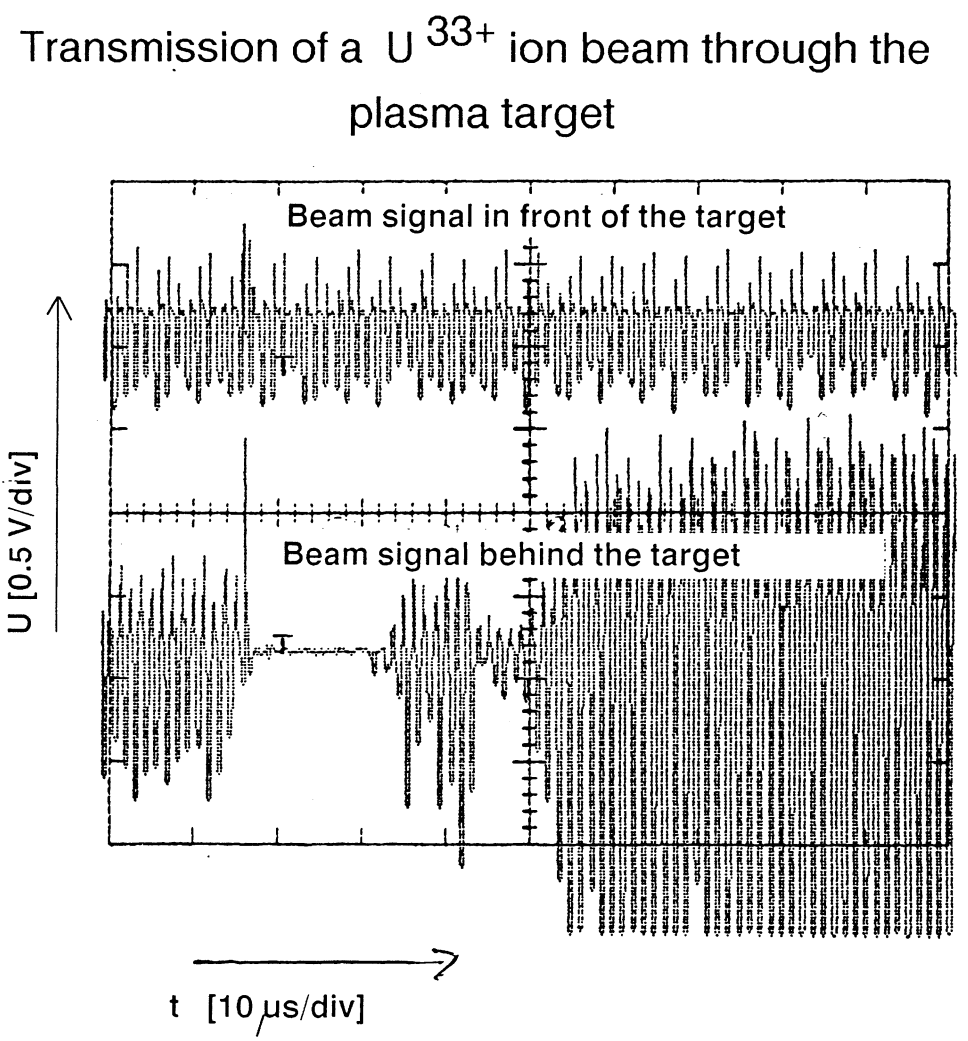

FIGURE 3 Plasma lens effect observed in the hydrogen discharge plasma. The beam intensity signal in front of the target is shown in the upper part, and the lower part of the picture shows the signal of the beam intensity traversing the plasma target.

of the ion beam available from the SIS. Recent experimental results[9] already demonstrated an effective plasma lens for heavy ions.

3 INTERACTION OF HEAVY IONS WITH IONIZED MATTER

The theoretical description of the energy loss of charged particles in cold, non ionized matter, is well established, well understood, and corroborated by a large number of experimental data during a number of decades. This is, however, not the case for hot

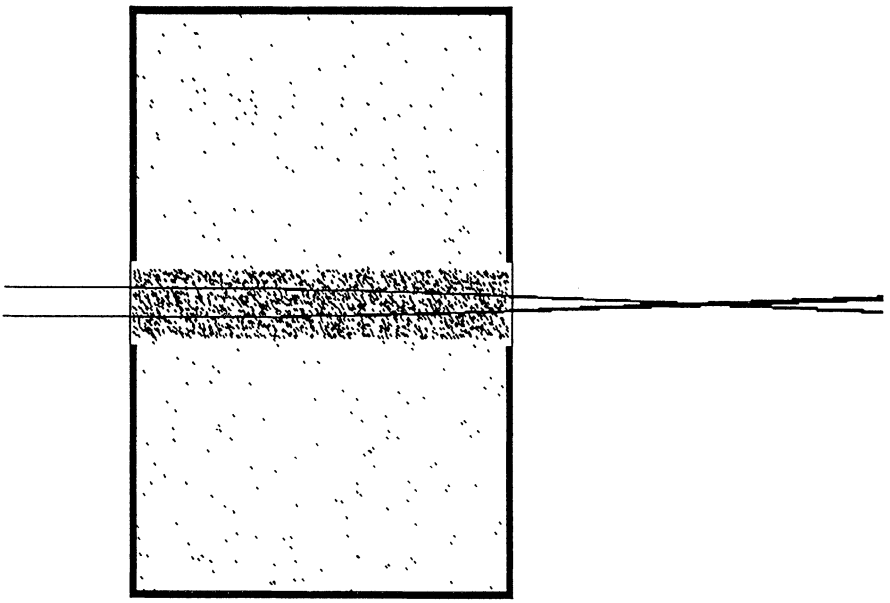

FIGURE 4 Focusing properties of the z-pinch plasma simulated by the Monte-Carlo code for a field gradient of 25 T/m, and an incident Argon beam at 11.4 MeV/u. The plasma density is $1.5\ 10^{19}\ \mathrm{cm}^{-3}$

ionized matter and existing theories have not yet been verified by experiments for a broad range of ion species. Moreover, the energy deposition of heavy ions is an important issue in the design of high gain fusion pellets for ion beam driven inertial confinement fusion (ICF).

When the ion velocity (v) is much larger than the thermal velocity of the free plasma electrons, an increase in stopping power is generally predicted[10,11], since the minimum energy transfer in a collision is no longer given by the average ionization potential ($\bar{I}$) but by the potential energy of the electrons in the Debye sphere. At high plasma temperatures, however, when the thermal electron velocity exceeds the projectile velocity, even a decrease of the stopping power combined with a large increase in range straggling is predicted [5].

3.1 Enhanced Stopping of Ions in Plasmas

In the energy regime considered in the experiments reported here (1.4–11 MeV/u) the well known Bethe formula without polarization correction and shell correction term describes the energy loss of non relativistic charged particles in a hydrogen plasma ($Z_2 = 1$) in the following form

$$-(dE/dx) = (Z_{\mathrm{eff}} e\omega/v)^2 \times \ln \Lambda, \tag{1}$$

where Z_{eff} is the effective charge of the ion while it traverses the target, e is the electronic charge and ω the plasma frequency, determined by the density of particles. For a cold target, where only bound electrons are present the argument of the

Coulomb logarithm Λ is given by

$$\Lambda_{\text{bound}} = 2mv^2/\bar{I} \tag{2}$$

This can be extended in a straightforward way to fully ionized material with free electrons using binary collision theory. The Coulomb logarithm in this case reads:

$$\Lambda_{\text{free}} = 0.764v/b_{\min}\omega \tag{3}$$

The minimum impact parameter $b_{\min}$ depends on the velocity of the ion. Since the electronic mass (m) is negligible compared to the heavy ion mass, the impact parameter is given by

$$b_{\min} = \max(e^2Z_{\text{eff}}/mv^2; \hbar/2mv). \tag{4}$$

For the conditions of our experiment at $E_0 = 1.4$ MeV/u ($v = 7.49\,\alpha c = 1.64 \times 10^9$ cm/s) $b_{\min}$ is always given by

$$b_{\min} = e^2Z_{\text{eff}}/mv^2 \tag{5}$$

due to the high charge state Z_{eff} of the incident ions, and thus we have

$$\Lambda_{\text{free}} = 0.764\ \text{mv}^3/Z_{\text{eff}}e^2\omega \tag{6}$$

The enhancement of the stopping power of fully ionized hydrogen due to the Coulomb logarithm effect is of the order of a factor of 2 for all heavy ions.

3.2 Model Description of the Heavy Ion Effective Charge State

The charge state of heavy ions passing through matter is fluctuating rapidly, due to ionization and electron capture processes. A dynamic equilibrium of these processes finally determines the effective charge state Z_{eff} which is one key parameter in Eq. 1, and it turns out to be a function of the target thickness (x), the ion velocity (v) and the temperature (T) of the target material ($Z_{\text{eff}} = Z_{\text{eff}}(x, v, T)$). For a complete evaluation of the energy loss equation (1), the x-dependence of Z_{eff} has to be analyzed. A detailed treatment of this problem is found e.g. in Ref. 13, 14. For our purpose we developed a Monte-Carlo code to track the development of the heavy ion effective charge state, as the projectile traverses the plasma target, and used the results as an input for the energy loss calculation. In this code we treated ionization processes due to collisions of the heavy ion projectile with bound and free target electrons, and target nuclei in the framework of the binary encounter model of Gryzinski[15].

The dominant electron capture process in our experiment was recombination by capture of bound electrons, and in the case of the fully ionized plasma target, radiative electron capture (REC). Dielectronic recombination processes are also considered by the code according to Ref. 13.

For highly charged ions as U^{33+} which we regard as our standard example, electron capture processes occur to states with high principal quantum numbers, which are difficult to treat. The Oppenheimer-Brinkmann-Kramers (OBK) approximation provides, however, a simple method to describe these processes. Since in this experiment we are dealing with a hydrogen target, we used the Nikolaev formula[16]

for K-shell electron transfer to a projectile state with principal quantum number n and performed a summation over all possible n-states up to the numerical convergence limit. The resulting cross sections are known to overestimate experimental data[17], and we therefore applied the Chan–Eichler scaling factor to the OBK cross section[18].

An empirical scaling rule for the electron capture cross section into highly charged ions described by Schlachter and coworkers[19] represents our data equally well and due to its parametrization is especially suited to be used in a computer code.

Figure 5 shows the experimental results for the energy loss of U ions in a low density plasma target. The calculation shown in this figure is the result of the Monte-Carlo code developed for this experiment and includes the three most important atomic cross sections for charge changing processes:

- Ionization by collisions with target ions and electrons[15]
- Recombination by capture of bound electrons, and[20]
- Radiative recombination of free electrons[21]
- Dielectronic recombination[7].

While the dashed lines represent the energy loss of Uranium ions, assuming a constant value of Z_{eff}, the full lines take into account the variation of the effective charge state, while the ion traverses the plasma target. It is an important feature of

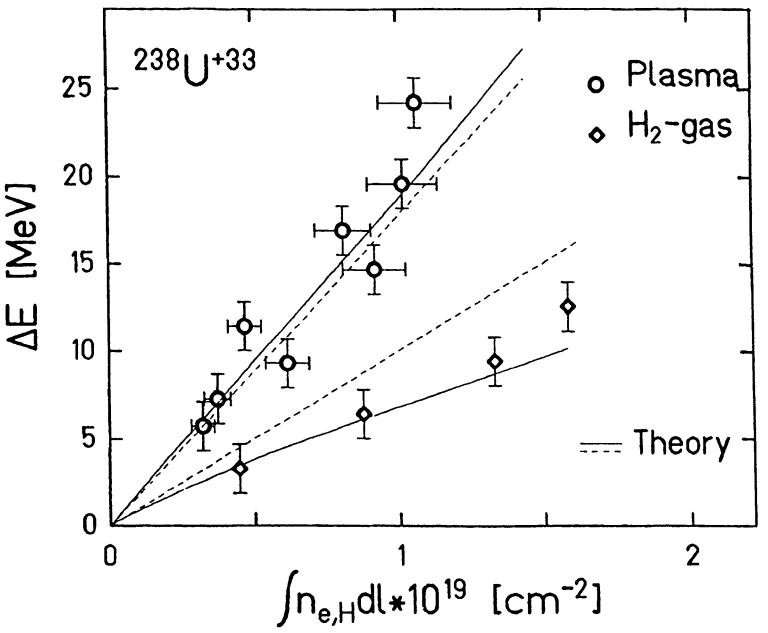

FIGURE 5 Comparison of experimental data from our stopping experiments to the result of the Monte-Carlo code to simulate the energy loss of heavy ions in a plasma target.

this experiment, that the ion charge state is initially above the equilibrium charge state in cold hydrogen gas. Therefore even in a target of low density ($n_e \approx 10^{17}$ cm^{-3}), as it was available for the first part of the experiment, the charge state of the ion starts to develop in opposite directions, depending on whether the target is cold hydrogen gas or a fully ionized plasma.

The energy loss data for cold hydrogen gas are well represented by the full curve, which takes into account, that the ion charge state drops from 33+ to the equilibrium value of 27+. Thus the deviation from the straight dashed line assuming a constant charge state of 33+ is quite obvious.

In the plasma case however our code predicts an increase of only one charge state, thus the full line (charge state variation) is still very close to the dashed straight line (constant charge state) and the experimental uncertainties do not allow to distinguish between these two cases. We therefore extended our measurements into the regime of a high density hydrogen plasma.

3.3 Energy Loss of Heavy Ions in a Dense Hydrogen Plasma

The z-pinch plasma target used in our experiment provides a fully ionized hydrogen plasma with free electron densities exceeding 10^{19} cm^{-3}. With this target we measured the energy loss of ^{208}Pb and ^{238}U ions at an energy of 1.4 MeV/u, and the charge state distribution of Ar ions ($E_0 = 4.8$ MeV/u) moving through the plasma. The z-pinch target was designed and constructed at the Fraunhofer-Institut für Lasertechnik in Aachen especially for the energy loss experiments[22]. The capacitor bank has a capacity of 4 μF and an inductance of 15 nH. It is typically charged to 20–40 kV corresponding to an energy of 0.8–3.2 kJ stored in the bank. The discharge vessel consists of a cylindrical quartz tube with a length of 20 cm and an inner diameter of 10.4 cm, with copper electrodes on both ends of the tube. It is filled with hydrogen at typical pressures of 0.5 to 3.5 mbars. Spark gaps are used as fast high power switches. After triggering the spark gaps the discharge starts at the inner surface of the quartz tube forming a hollow plasma cylinder. Driven by the strong azimuthal magnetic field generated by the high axial current (typically 400 kA) the plasma is compressed onto the axis, where in the pinch phase a very dense and hot plasma column with a diameter of about 10 mm is formed.

The time interval from ignition to the pinch phase is about 1.2 μs. It is followed by an expansion of the plasma where with 1 μs the plasma density decreases from above 10^{19} cm^{-3} to 10^{17} cm^{-3}. Measuring the energy loss during this time interval allows us to obtain energy loss data for a wide density range in one experiment.

The z-pinch has been integrated to the beamline of the UNILAC accelerator with a differential pumping system. The experimental setup is shown in Figure 6. With the magnetic analyzer turned off, energy loss measurements with time of flight technique are performed. The magnet serves for charge state analysis of the beam passing through the plasma. The beam passes through the tube on the axis of symmetry through small (3 mm diameter) apertures in the electrodes.

In Figure 7 we present the results of the energy loss measurement as a function of time (upper part of Figure 7) together with the light output signal of the plasma

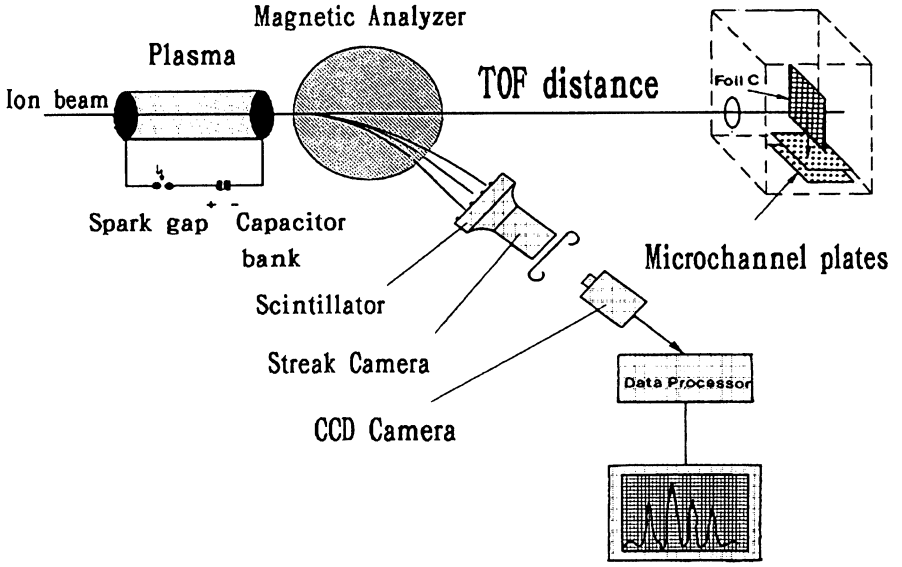

FIGURE 6 Experimental set-up.

(lower part of Figure 7). Up to 600 ns the data correspond to the energy loss (2 MeV) in the cold hydrogen gas target (length = 20 cm, p = 2.5 mbar). At that point the pinch reaches the beam axis and the target density and the associated energy loss rises steeply, exceeding the range accessible to our time-of-flight spectroscopy.

The plasma light signal is measured through the exit aperture of the z-pinch cathode, thus the line of sight for this signal is along the beam plasma interaction zone at the center of the pinch column. The intensity of this signal is correlated to the free electron density of the plasma and therefore it shows the same features as the energy loss measurements, with a very steep rise of the intensity, when the pinch collapses on the axis. At this time the plasma density is above 5×10^{18} cm^{-3} and the ions are stopped completely inside the plasma column and a time of flight energy measurement is no longer possible. This explains the lack of energy loss data between 0.8 μs and 1.2 μs in the upper part of Figure 7. During the expansion phase of the pinch the energy loss is again within the limits accessible for time-of-flight spectroscopy and we observe an energy loss corresponding to 45% of the incident beam energy of 291 MeV.

The experiment consisted of two parts: Measurement of the energy loss of heavy ions and diagnostics of the plasma density and temperature. The energy loss was determined with a time-of-flight method using a 430 cm time-of-flight distance. The time resolution achieved was 2 ns corresponding to an accuracy of the energy loss measurement of ± 2 MeV for Pb ions. With this system energy losses up to 45% of the incident energy could be detected.

The plasma density diagnostics were performed with laser interferometry in Mach-Zehnder geometry along the z-pinch axis.[23] On-axis interferometry gives the

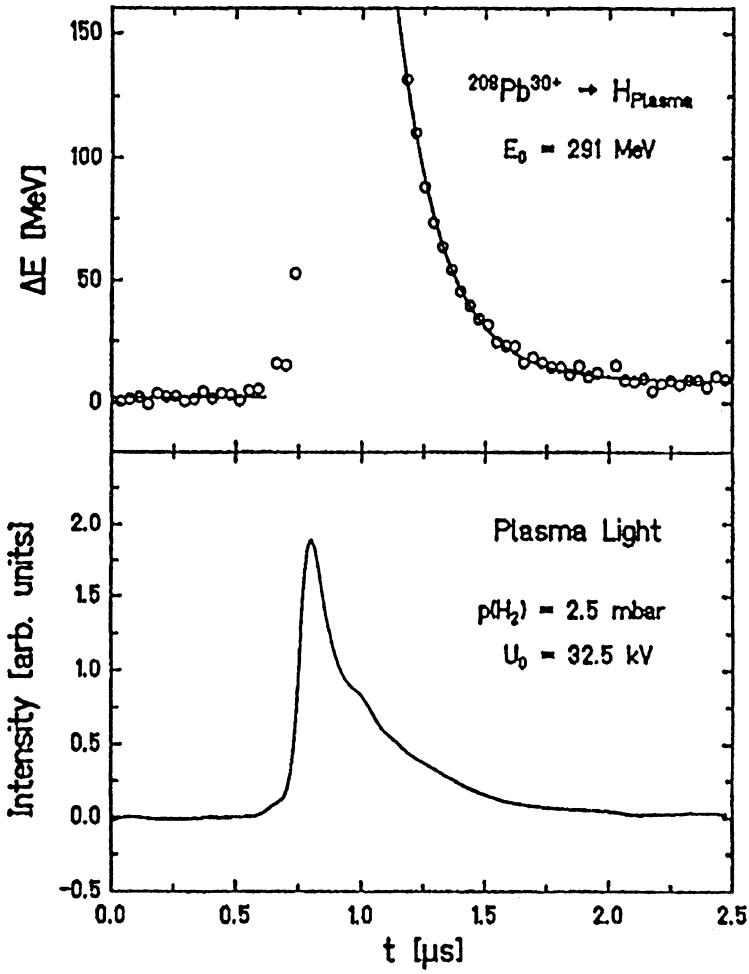

FIGURE 7 Time dependence of the energy loss (upper part) and the corresponding light emission from the plasma target (lower part).

most accurate information about the quantity $\int n_e \, dl$ e.g. the free electron density integrated along the interaction zone of ion beam and plasma. With this method area densities up to $5.2 \times 10^{19}\,\mathrm{cm}^{-2}$ could be diagnosed with an error of $\pm 1.5 \times 10^{18}\,\mathrm{cm}^{-2}$. In the phase of higher plasma density this diagnostic technique fails because the laser light is absorbed in the plasma. The plasma temperature was determined by spectroscopy of the emitted light, analyzing the H_α emission. In the pinch phase it is above 5 eV. During the following expansion phase temperature decreases but for several microseconds stays high enough to guarantee a degree of ionization of more than 99%. Thus the shown energy loss data were all obtained in a completely ionized plasma.

In Figure 8 the measured energy loss of $^{208}Pb^{30+}$ ions is displayed as a function of the free electron area density. The given error bars represent the full error comprising the error of the energy loss measurement the error of the interferometry and the uncertainty in matching the time scale of both. The energy loss for cold hydrogen gas is derived from tables.[24] The observed energy loss in the plasma is by a factor of three higher than the energy loss in cold gas.

We compare the data to our calculation. The ion charge state in the plasma increases because the dominant electron capture process in cold matter e.g. the capture of bound electrons is strongly suppressed in a highly ionized plasma. Our calculation predicts an increase of the Pb ion charge from 30+ to 38+ causing the energy loss to rise stronger than in the case of a constant charge state. Note that the theoretical curve has an ascending slope. The agreement of the calculation with the experimental data is very good, also for the ^{238}U data not shown here.

First experiments to measure the charge state distribution (Figure 9) of an Ar beam passing through the plasma have been performed. The initial charge state is 10+ or 15+ at an energy of 4.8 MeV/u. We observe that the beam is almost completely stripped into charge state 16+, a He-like configuration regardless of the initial charge state. Dielectronic recombination processes prevent the ions from being ionized into higher charge states and a very narrow charge state distribution centered at Ar^{16+} is the observed result.

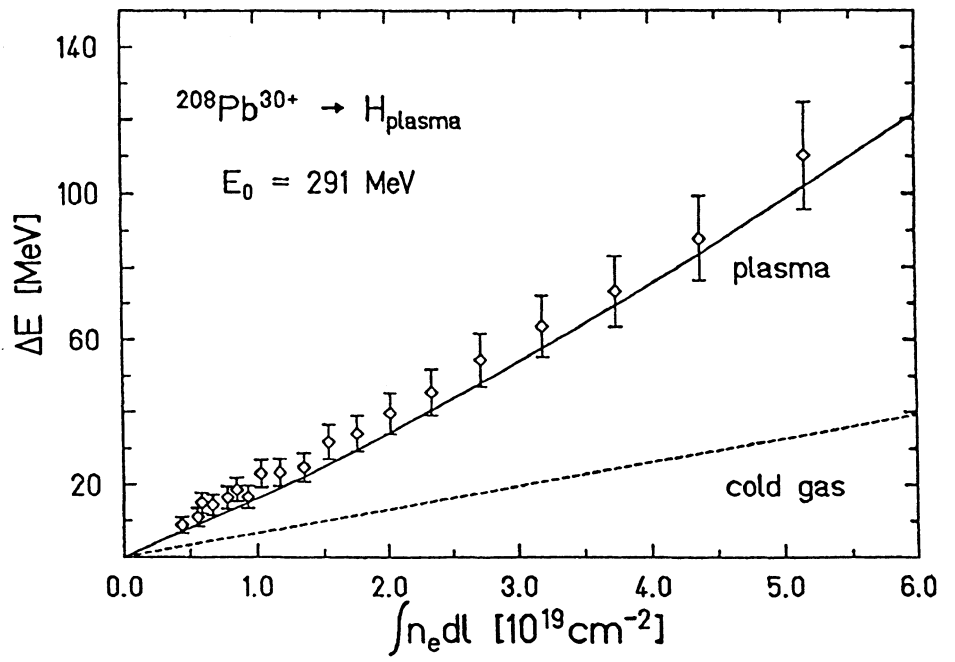

FIGURE 8 Energy loss of Pb ions in a dense hydrogen plasma.

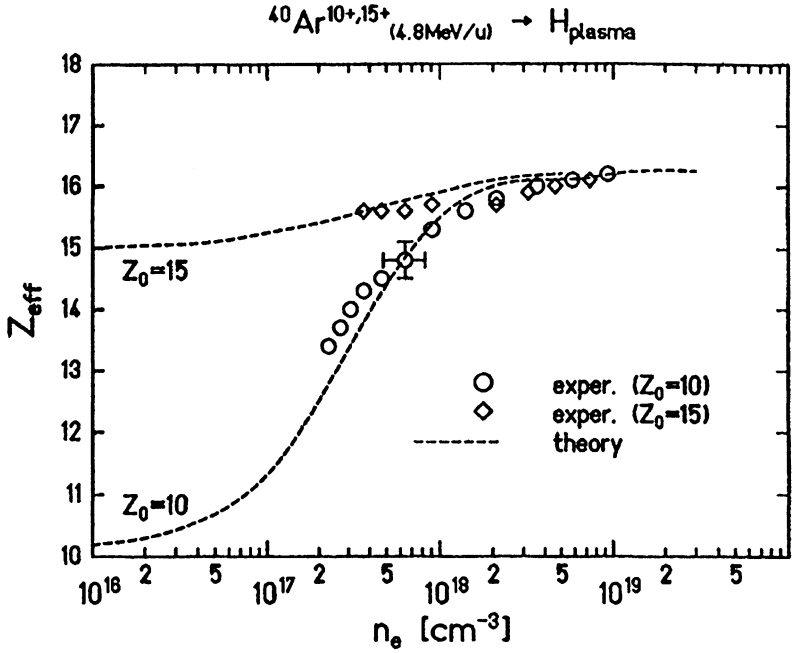

FIGURE 9 The effective (average) charge state of Ar ions traversing the plasma target.

ACKNOWLEDGMENT

The experiments reported here are performed at GSI in an international collaborative effort of a number of institutes including also MPQ-Garching, TH Darmstadt, IPN Orsay, GREMI-CNRS Orleans, LPGP Orsay, FHG-ILT Aachen, Univ. Giessen, and ITEP Moscow.

The funding for the German institutes collaborating with GSI in this experimental program was provided by the federal ministry for research and technology (BMFT).

REFERENCES

1. C. Rubbia, *Nucl. Instr. and Meth. A* **278**, 253 (1989).
2. E. Storm, Laser Interaction with Matter, eds.: G. Velarde, E. Minguez, J. M. Perlado, ECLIM Madrid 1988, p. 85.
3. D. H. H. Hoffmann, J. Meyer-ter-Vehn, R. W. Müller, I. Hofmann, R. Bock, and R. Arnold, *Nucl. Instr. Meth. A* **278**, 44 (1989).
4. K. Blasche, and E. Franczak, GSI Nachrichten 12–89 (1989).
5. J. Jacoby, D. H. H. Hoffmann, R. W. Müller, K. Mahrt-Olt, R. C. Arnold, V. Schneider, and J. Maruhn, *Phys. Rev. Lett.* **65**, 2007 (1990).
6. B. Heimrich, H. Nestle, M. Winkler, D. H. H. Hoffmann, and H. Wollnik, *Nucl. Instr. Meth. A* **294**, 602 (1990).
7. H. Wollnik, J. Brezina and M. Berz, *Nucl. Instr. Meth. A* **258**, 408 (1987).
8. D. Gadés, R. Bimbot, S. Della-Negra, M. Dumail, B. Kubica, A. Richard, M. F. Rivet, A. Servajean, C. Fleurier, A. Sanba, C. Deutsch, G. Maynard, D. H. H. Hoffmann, K. Weyrich, and H. Wahl *Europhys. Lett.* **8**, 701 (1988).

9. E. Boggasch, Proc. Int. Symp. on Heavy Ion Inertial Fusion, Monterey, 1990.
10. T. A. Mehlhorn, *J. Appl. Phys.*, **52** 6522 (1981).
11. C. Deutsch, P. Fromy, X. Garbet, G. Maynard, *Fus. Technol.* **13** 362 (1988).
12. M. M. Basko, Sov. J. Plasma Phys. **10**, 689 (1984) [*Fiz. Plazmy* **10** 1195 (1984)].
13. Th. Peter, and J. Meyer-ter-Vehn, Phys. Rev. A (1990) in print and Th. Peter, diploma thesis (1985), University of Munich, 1985.
14. Th. Peter, R. Arnold, J. Meyer-ter-Vehn, *Phys. Rev. Lett.* **57** 1859 (1986).
15. M. Gryzinski, *Phys. Rev.* **A138** 305 (1965).
16. V. Nikolaev, *Zh. Eksp. Theor. Fiz.* **51** 1263 (1966).
17. A. M. Halpern, J. Law, *Phys. Rev.* **31** 4 (1973).
18. LF. T. Chan, J. Eichler, *Phys. Rev. Lett.* **42** 58 (1979).
19. A. S. Schlachter, J. W. Stearn, W. G. Graham, K. H. Berkner, R. V. Pyle, and J. A. Tanis, *Phys. Rev.* **A27**, 3372 (1983).
20. J. R. Oppenheimer, *Phys. Rev.* **31**, 349 (1928).
21. J. L. Spitzer, *Astrophys. J.* **107**, 7 (1948).
22. R. Noll, H. Kunze, C. R. Haas, Nucl. Instr. and Meth. A 278, 85 (1989).
23. H. Kunze, R. Noll, C. R. Haas, M. Elfers, J. Hertzberg, and G. Herziger, Laser Part. Beams **8**, 595 (1990).
24. L. C. Northcliffe, and R. F. Schilling, *Nucl. Data Tables A7*, 223 (1970).